Micro sliding friction model considering periodic variation stress distribution of contact surface and experimental verification

Sheng-Hao Lu(卢晟昊), Jing-Yu Han(韩靖宇), and Shao-Ze Yan(阎绍泽)†

State Key Laboratory of Tribology, Department of Mechanical Engineering, Tsinghua University, Beijing 100084, *China*

(Received 16 June 2022; revised manuscript received 26 August 2022; accepted manuscript online 8 September 2022)

Micro sliding phenomenon widely exists in the operation process of mechanical systems, and the micro sliding friction mechanism is always a research hotspot. In this work, based on the total reflection method, a measuring device for interface contact behavior under two-dimensional (2D) vibration is built. The stress distribution is characterized by the light intensity distribution of the contact image, and the interface contact behavior in the 2D vibration process is studied. It is found that the vibration angle of the normal direction of the contact surface and its fluctuation affect the interface friction coefficient, the tangential stiffness, and the fluctuation amplitude of the stress distribution. Then they will affect the change of friction state and energy dissipation in the process of micro sliding. Further, an improved micro sliding friction model is proposed based on the experimental analysis, with the nonlinear change of contact parameters caused by the normal contact stress distribution fluctuation taken into account. This model considers the interface tangential stiffness fluctuation, friction coefficient hysteresis, and stress distribution fluctuation, whose simulation results are consistent well with the experimental results. It is found that considering the nonlinear effect of a certain contact parameter alone may bring a greater error to the prediction of friction behavior. Only by integrating multiple contact parameters can the accuracy of friction prediction is improved.

Keywords: periodic variation stress distribution, micro sliding friction model, tangential stiffness, experimental analysis, stick-slip

PACS: 46.55.+d, 42.30.Va, 78.20.Ci **DOI:** 10.1088/1674-1056/ac9043

1. Introduction

The distribution of interface contact stress has an important influence on the friction behavior of the interface, with the vibration phenomenon considered. However, vibration analysis mainly focuses on the solution of higher-dimensional differential equations, but less attention is paid to the interface contact friction model used in vibration analysis. The current research generally adopts the simple Coulomb friction model without considering the nonlinear influence of contact interface parameters. When the tangential force of the interface moves back and forth, the interface will fluctuate back and forth correspondingly, which is called micro sliding friction. Micro sliding friction is a kind of stick-slip motion with historical memory considering the fluctuation amplitude. Under the cyclic action of force, the load-deformation curve of the structure is called the hysteretic curve. It reflects the deformation characteristics, stiffness degradation, and energy consumption of the structure in the process of repeated stress. It is the basis for determining the restoring force model and nonlinear seismic response analysis. The hysteretic curve is also called restoring force curve. It contains many important friction characteristics, which can make the friction model predict the hysteretic curve more accurately. The research on the influence of contact parameters on damping and energy dissipation in micro sliding friction has important engineering application value.

Because interface damping is sensitive to many physical parameters, such as elasticity, roughness, contact geometry, and load distribution, it is difficult to predict and control interface damping. The study about the influence of physical parameters on energy dissipation is of great significance in improving the prediction accuracy of interface damping. It is generally believed that the aspect ratio is negatively correlated with energy dissipation, but the normal force fluctuation amplitude,[1,2] the tangential force fluctuation amplitude,[2] the contact area,[3] and the friction coefficient[3,4] are positively correlated with energy dissipation. Owing to the complexity of contact behavior, the explanations of the influence mechanism of some parameters on energy dissipation are inconsistent.[5] Gu and Xu[3] adopted a three-dimensional (3D) numerical friction contact model and considered that the tangential stiffness is positively correlated with energy dissipation. Xiao *et al.*[6] used a combination of the shear layer model and finite element method for analysis. It is found that although the tangential stiffness increases the length of the slip zone, the displacement amplitude is small and the energy dissipation is reduced, so the tangential stiffness is negatively correlated with the energy dissipation. In addition, it has been found that there is a power-law relationship between the energy dissipation and tangential fluctuation amplitude,[2,6,7] but

†Corresponding author. E-mail: yansz@mail.tsinghua.edu.cn

© 2023 Chinese Physical Society and IOP Publishing Ltd

the determination of the power-law index is still controversial. Goodman[7] thought that the power-law index is 3, and Usta *et al.*[2] thought that the power-law index is 2.49. However, Xiao *et al.*[6] thought that the power-law index is not a fixed value, but related to the stress distribution. Through theoretical analysis and finite element modeling, it has been confirmed that the stress distribution at the contact interface significantly affects nonlinear characteristics such as damping.[8] Sandia laboratory[9] found that the shape of the contact sample will be affected by the edge stress effect, which will influence the prediction of structural dynamic performance. In the vibration response analysis of shrouded blade dampers, Two kinds of test-beds have been developed based on the experimental object. One is shape simulation, which is analyzed by the experimental scheme of equal-size scaling. For example, the shock absorber test bench has been designed.[5,10,11] To minimize the false response, better control of the experimental setting, and simplification of the test process, the design scheme of a static bench was adopted.

It is found that for high-frequency excitation, the sensitivity of the model to contact stiffness is low, but at low excitation, the contact stiffness will affect the accuracy of the model (with an error of 1%). The second is functional simulation. The interface micro sliding friction behavior is simulated by coupling multiple exciting forces. For example, in the 2D friction test system designed by Asai and Gola,[12] it is found that the alternating friction coefficient is the key parameter to determine the change law of energy dissipation. Through finite element analysis, Asai and Gola[12] believed that this may be related to the uneven stress distribution caused by the normal force fluctuation. However, due to the measurement technology, the dynamic change of interface stress distribution cannot be obtained, so this conclusion has not been confirmed experimentally.

It is very important to use appropriate contact analysis technology to measure the stress distribution of the contact interface, but the contact interface is closed, it is difficult to observe directly, and the dynamic observation is more difficult.[13] The optical method is the longest used in the study of contact distribution visualization.[14,15] As a non-contact dynamic measurement technology, the optical method can realize the visual observation of contact distribution of contact interface on different scales from submicroscopic to macroscopic, which can be used to characterize the change of interface stress distribution, and plays a more and more important role in revealing the evolution law of interface contact behavior.[16] The generation mechanism of stick-slip was studied based on the total reflection method and applied to earthquake early warning.[17–21] The variation law of precursor wavelength in the preslip stage in stick-slip friction was analyzed, with the influence of contact angle and sample size considered.[22–24] Nano scale stick-slip behavior is also a hot topic in recent years. Lee *et al.*[29] studied the anisotropic nanoscale and sub-nanoscale friction behaviors between phosphorene and silicon tip. Tian *et al.*[30] clarified stick-slip instabilities for interfacial chemical bond-induced friction on a nanoscale. The influence of environment, temperature, oxidation, three body, wear, and plastic deformation on the contact interface lead to a complex contact behavior,[16] which brings challenges to the prediction of contact behavior. Considering the actual working conditions, it is very meaningful work to reveal the "black box" behavior in interface contact.

In this work, based on the total reflection method, the dynamic stress distribution is considered in the friction phenomenon for the first time, and the 2D vibration contact behavior of the contact interface is analyzed experimentally. Through the analysis of contact behaviors under different vibration angles, a more accurate nonlinear contact parameter model is established, and the friction model can improve the accuracy of vibration response prediction. The remainder of this paper is as follows. In Section 2, we develop a 2D vibration experimental device based on the total reflection method. In Section 3, we analyze the 2D vibration friction behavior of polymethyl methacrylate (PMMA) material experimentally, with the normal force fluctuation considered. In Section 4, the influence of vibration angle on the micro sliding behavior of interface is studied in experiment, and the influence of vibration angle on the force and displacement in the micro sliding behavior are analyzed. and we establish the micro sliding friction model, with the interface stress distribution fluctuation considered. In Section 5 some conclusions are drawn from this study.

2. Experiment method

2.1. Experimental principle

It is assumed in the general vibration analysis that the excitation is used in the normal or tangential direction of the contact interface as shown in Fig. 1(a), the specimen 2 is fixed, and the fixed normal force F_n and the fluctuating sinusoidal tangential force F_t are both applied to the specimen 1. Besides, the displacement δ of specimen 1 fluctuates back and forth along the direction x, δ, and F_t forming a symmetrical hysteretic curve about the original point as shown in the black curve in Fig. 1(b). In practical engineering, the contact surface is excited by inclined vibration due to uneven contact or external excitation.

As shown in Fig. 1(c), the angle between the summation of forces and the x direction is α, the specimen 2 is fixed. The fixed normal force F_n and the fluctuating sinusoidal tan-

gential force F_t are applied to specimen 1, respectively. The displacement δ of specimen 1 fluctuates back and forth along the direction x, but the hysteresis curve formed by δ and F_t is no longer symmetrical about the origin as shown in the red curve in Fig. 1(b). The motion in Fig. 1(c) can be equivalent to that in Fig. 1(d). When there is an angle between the excitation and the interface, it can be equivalent to a 2D coupling excitation with a fluctuating normal force and a fluctuating tangential force applied to the contact interface. Among them, the initial value of the tangential forceF_t is $F_{t,m}$, the amplitude is $F_{t,a}$, and the initial value of the normal force F_n is $F_{n,m}$, the amplitude is $F_{n,a}$.

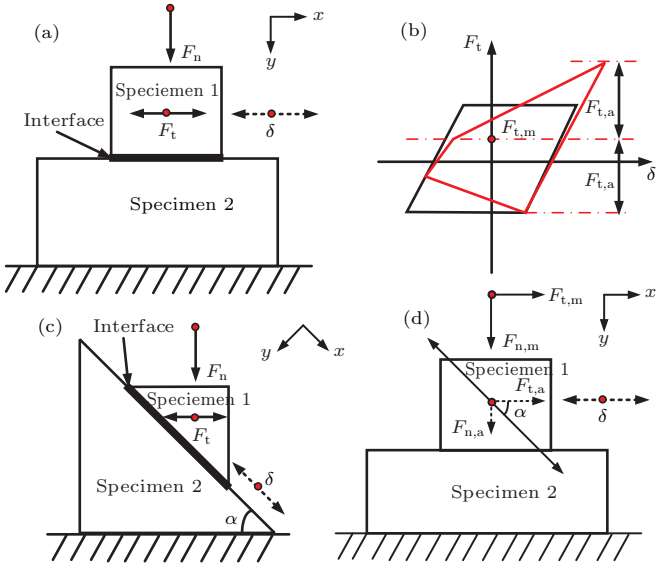


Fig. 1. Schematic diagram of tilting vibration.

2.2. Experimental device overall design

Referring to Asai *et al.*'s[12] experimental scheme and the total reflection method, a 2D vibration experimental system is built, which can simultaneously collect the displacement, contact force, and contact image of the contact interface as shown in Fig. 2. The experimental system consists of a control system, actuator, and signal acquisition system. The control system is mainly composed of a computer, signal generator, and driving power supply. The computer adjusts the amplitudes, frequencies, and phases of the two signals through the signal generator, and drives the actuator after being amplified by the driving power supply (output voltage 0 V–150 V, frequency 2 Hz–100 Hz). The actuator consists of two piezoelectric actuators and two flexure hinges. The piezoelectric actuator is used to fluctuate normal force and tangential force to the contact specimen through the flexure hinge to drive the contact interface to move in a predetermined way. The piezoelectric actuator adopts the Core Tomorrow's PST150/14/120VS20 (stroke 125.616 μm, stiffness 35 N/ μm, capacitance 47 μF). The driving voltage is 0 V–150 V, the single-channel driving frequency range is 0.01 Hz–100 Hz, and the dual-channel driving frequency range is 2 Hz–100 Hz. Because the piezoelectric stack cannot bear the tensile force, a spring plate is installed in the ceramic package to achieve the purpose of preloading, and the preloading force is 10% (470 N) of the maximum force. The signal acquisition system consists of two laser displacement sensors, six-dimensional (6D) force sensors and two tangential force sensors, a high-speed camera, and laser. It is used to collect the contact force, displacement, and contact area images of the contact interface fluctuation in real-time. By analyzing their evolution, the mechanism of micro sliding contact behavior considering 2D vibration can be analyzed.

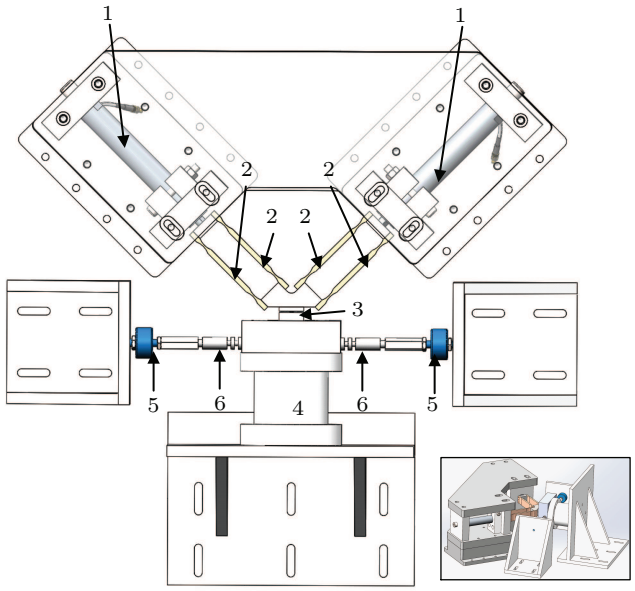


Fig. 2. Schematic diagram of 2D vibration test bench. 1: piezoelectric actuator, 2: flexure hinge, 3: specimen group, 4: six-dimensions force sensor, 5: force sensor 1, and 6: rod and shaft.

2.3. Acquisition and analysis of signals

The force and displacement acquisition equipment mainly includes two twin-screw force sensors, a six-component 3D force sensor, two laser displacement sensors, optical fiber displacement sensor, and signal acquisition device.

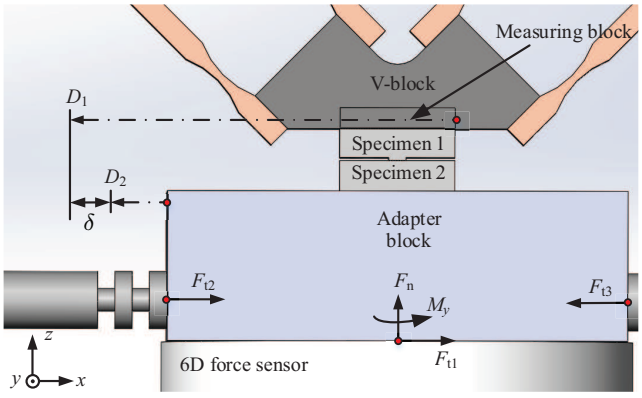


Fig. 3. Measurement of force and displacement.

It can be seen from Fig. 3 that the tangential force F_t on the interface is composed of three components F_{t1}, F_{t2}, and F_{t3}. The micro force sensor is used to measure the tangential component forces F_{t2} and F_{t3}, the 3D force sensor is used to measure the normal force F_n, the tangential component force F_{t1}, and the torque M_y. Because of the large size of the laser displacement sensor, we use the indirect measurement method. The measuring block is fixedly connected with the V-block through the super glue. Since specimen 1 is fixed on the V-block, the displacement of the measuring block is used as the displacement D_1 of specimen 1. The displacement of the adapter block is taken as the displacement D_2 of specimen 2 and the relative displacement of the interface. The main parameters of measuring equipment are shown in Table 1.

According to the above methods, the tangential force F_t and relative displacement δ of the interface during the experiment are obtained. Figure 4 shows a hysteresis curve consisting of F_t and δ. The hysteresis curve shows a periodic motion of the contact interface. F_t gradually increases along A–B–C–D, which is regarded as the forward section; F_t gradually decreases along D–E–F–A, which is called the negative segment. According to the various characteristics of the hysteresis curve, it can be divided into the following stages: positive viscous section (AC) to positive sliding section (CD), and negative viscous section (DF) to negative sliding section (FA). The state transition points are A, C, D, and F, respectively. During the experiment, the tangential force changes periodically, $F_{t,a}$ is the amplitude of tangential force fluctuation, the slope of the initial section of positive viscous is defined as positive tangential stiffness $K_{t,p}$, and the slope of the initial section of negative viscous is defined as negative tangential stiffness $K_{t,n}$. When $F_t = 0$ N, the difference between the relative displacements of the positive section and the negative section is called sliding distance d_{slip}, the area around the hysteresis curve is called energy dissipation E_D.

Table 1. Main parameters of measuring equipment.

Equipment	Model	Parameter
Force sensor with twin-screw	BUFSON BSLM-3	accuracy/range: 0.5 N/500 N
Six-component three-dimensional force sensor	BUFSON BSfY-3	accuracy: 0.1% $F_x = F_y = 500$ N range: $F_z = 500$ N $M_x = M_y = 10$ Nm
Laser displacement sensor	KEYNCE LK-H020	accuracy/range: 1 μm/5 mm
Signal collector	ECON	channel: 32 sampling frequency: 100 kHz

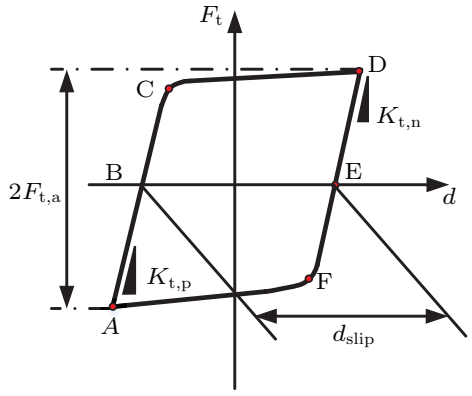


Fig. 4. Schematic diagram of hysteresis between F_t and δ.

2.4. Test specimen and total reflection method

The specimen group consists of the specimen 1 and the specimen 2. The interface is rough and smooth, respectively, and the specimen material is polymethyl methacrylate (PMMA). The specimen 1 has a double boss structure as shown in Fig. 5(a). The convex plate size ($x \times y \times z$) is 3 mm×1 mm×0.5 mm, the upper surface of the convex is sandblasted (elastic modulus: 3.16×10^9 Pa, roughness: 2.9 μm) as shown in Fig. 5(a), and the bottom size ($x \times y \times z$) of specimen 1 is 20 mm×19 mm×4.5 mm. Specimen 2 is a rectangular block as shown in Fig. 5(c), the size ($x \times y \times z$) is 20 mm×19 mm×4.5 mm, and the surface is smooth (0.002 μm Sq), the surface morphology is shown in Fig. 5(d).

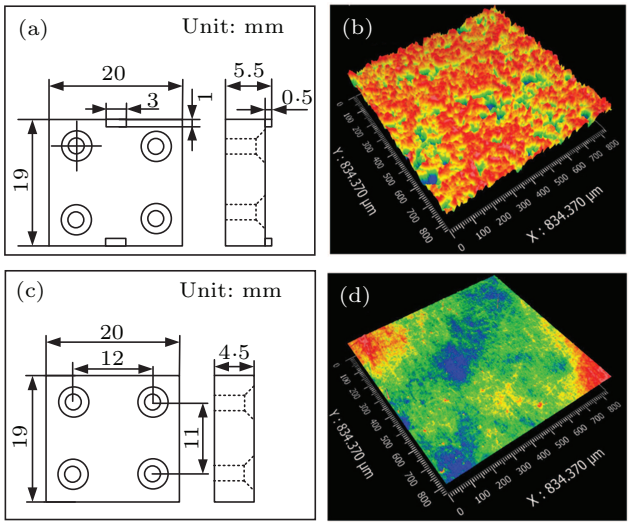


Fig. 5. Specimen group: (a) size of specimen 1, (b) rough surface, (c) size of specimen 2, and (d) smooth surface.

The image of the contact area is collected based on the total reflection method[26,27] as shown in Fig. 6(a). When the laser is injected into specimen 1 from the side, the smooth surface of specimen 2 is totally reflected when specimen 1 does not contact specimen 2, and there is no spot image on the contact interface. When the asperities on the rough surface contact the smooth surface, diffuse reflection occurs in the micro-contact area. During the experiment, the camera collects the contact area image at the frequency of 60 Hz. Figure 6(b) shows the contact images observed before and after the contact. Because the camera is at 64°, the image in the y direction becomes 3.5 times smaller. Extract the intensity matrix $I(x,y,t)$ of the gray image of each frame in the video, then x and y will be the positions of the pixels in the matrix. The contact image intensity $I(x,y,t)$ at time t is expressed as[28]

$$I_{\text{sum}}(t) = \sum_{x=1}^{n}\sum_{y=1}^{m} I(x,y,t), \tag{1}$$

where m and n are the row and column sizes of the image intensity matrix.

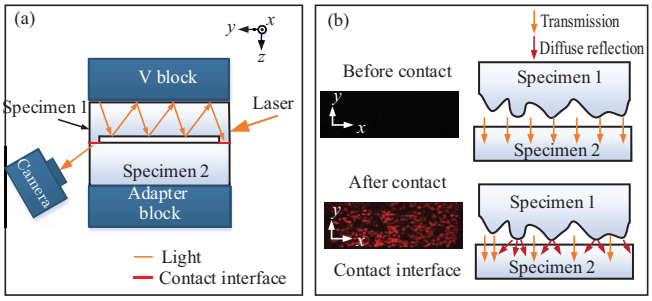


Fig. 6. Principle diagram of total reflection method: (a) light path diagram, (b) principle of the total reflection method.

Considering that the whole and local contact image intensity have a good linear relationship with the normal force, the change of the contact image intensity distribution is approximately consistent with that of the real contact area distribution in the stick-slip process. It is found that the change of contact area in the process of stick-slip is mainly in the x direction. The intensity distribution $I(x,t)$ in the x direction is obtained by summing the intensity of the contact image in the y direction, as shown below:

$$I(x,t) = \sum_{y=1}^{m} I(x,y,t). \tag{2}$$

The change of contact area distribution in x direction on the equivalent interface is adopted.[28]

Assuming that the change of the real contact area and the normal force are both linear, the distribution of the $F_{\text{n,m}} = 58$ N contact area on the interface can approximately represent the distribution of the interface stress. The equivalent stress distribution $\bar{P}(x,t)$ along the x direction of the interface is expressed as follows:

$$\bar{P}(x,t) = \frac{\sum_{y=1}^{m} I(x,y,t)}{\sum_{y=1}^{m} I(x,y,0)}. \tag{3}$$

3. Influence of normal force fluctuation on micro sliding friction behavior

3.1. Micro sliding friction behavior in constant normal force experiment

When $F_{\text{n,a}} = 0$, $F_{\text{t,m}} = 0$, and the normal excitation is a constant, the tangential force $F_{\text{t,a}}$ increases by increasing or reducing $F_{\text{V,a}}$ and $F_{\text{H,a}}$, which is used to analyze the influence of tangential force amplitude on the interface micro sliding behavior. This experiment is called constant normal force experiment. The excitation frequency is 2 Hz, and the changes of contact force, displacement, and contact image are measured in real-time. The dynamic stress distribution is used to analyze the micro sliding friction behavior.

The experiment has good repeatability, the relative error is less than 2.13%. Figure 7(a) shows the time history curve of F_{t}, F_{n}, δ in one cycle when $\delta_{\text{a}} = 16$ μm. With the increase of the tangential force (blue dotted line), the relative displacement increases gradually. When F_{t} increases to 19 N, F_{t} is larger than the friction force, the interface slides forward (CD segment), and the relative displacement continues to increase, but F_{t} remains unchanged. When δ increases to 17 μm, it reaches the maximum point, F_{t} begins to decrease, and the interface has a negative stick (DE segment). When the tangential force gradually decreases to −18 N, the interface has a negative slip (EF segment). The change of a tangential force and relative displacement of one cycle can form a closed hysteretic curve. Figure 7(b) shows the hysteretic curves under different relative displacement amplitudes δ_{a}. When $F_{\text{t,a}}$ is less than the maximum static friction (19 N), there is no macro sliding on the interface, and the tangential force amplitude increases with the increase of $F_{\text{t,a}}$. When $F_{\text{t,a}}$ is larger than the maximum static friction, the interface has a positive slip. With the increase of relative displacement amplitude, the tangential force amplitude will not increase, and the slip distance d_{slip} and energy dissipation E_{D} will also increase gradually. Figures 7(c) and 7(d) show the relationship between δ_{a} and d_{slip} under different normal forces, and the relationship between δ_{a} and E_{D}. Both E_{D} and d_{slip} are related to δ_{a}. The value of d_{slip} decreases with the increase of normal force, but the correlation of E_{D} with normal force is small. When the relative displacement amplitude is the same, although the increase of normal force leads d_{slip} to decrease, the increase of tangential force amplitude compensates for the loss, and thus ensuring that the area basis enclosed by the hysteresis curve remains unchanged.

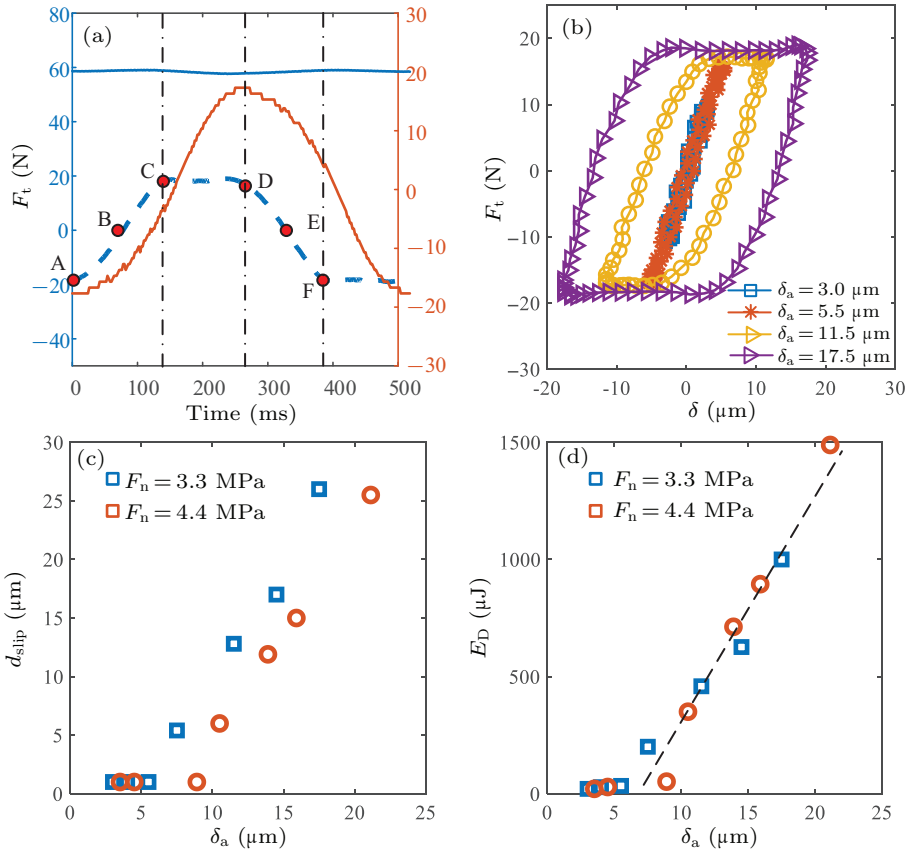


Fig. 7. Experimental results of constant normal force. (a) Time history curve of one cycle of F_t, F_n, and δ; (b) hysteretic curves of different values of δ_a; (c) relation curves between δ_a and d_{slip} for different values of F_n; and (d) relation curve between δ_a and E_D.

3.2. Micro sliding friction behavior in variable normal force experiment

When $F_{t,a} = F_{t,a}$, the vibration angle is 45°, and $F_{n,m}$ is fixed. When $F_{t,a}$ changes, the interface will be affected by the fluctuation of normal force and tangential force. This experiment is called the variable normal force experiment. Figure 8(a) shows the time history curve of one cycle of tangential force F_t, normal force F_n and relative displacement δ corresponding to $F_{n,m} = 60$ N. The relative displacement increases with the increase of the tangential force (blue dotted line). When the tangential force increases to 13 N (D point), the tangential force is greater than the maximum static friction force, and the interface slips (CD segment). Unlike Fig. 7(a), the tangential force and relative displacement continue to increase, but the growth rate of the tangential force slows down. This is mainly due to the increase of interface friction caused by the continuous increase of normal force at this stage. When the relative displacement increases to 17 μm, it reaches the maximum point and then F_t begins to decrease, and the negative stick (DE segment) occurs at the interface. When the tangential force gradually decreases to −14 N, the negative slip (EF segment) occurs at the interface. Because the normal force decreases gradually at this stage, the absolute value of the tangential force decreases gradually. Compared with the result of constant normal force experiment, the extreme value of tangential force increases in the positive section and decreases in the negative section, resulting in the whole hysteretic curve that is no longer symmetrical about the center point, then $F_{n,m} \neq 0$. This means that when the normal force fluctuates, one side of the contact interface will bear more shear force. Figure 8(b) shows the hysteretic curves with different values of δ_a. When $F_{t,a}$ is less than the maximum static friction, there is no macro slip on the interface, and the tangential force amplitude increases with the increase of $F_{t,a}$. When $F_{t,a}$ is greater than the maximum static friction, the interface will slide macroscopically. With the increase of δ_a, the tangential force amplitude $F_{t,a}$ and d_{slip} increase gradually. The maximum tangential force increases gradually, while the minimum value remains stable, which indicates that the increase of d_{slip} will lead the side of the interface to bear a larger shear force more severe. Figure 8(c) shows the logarithmic relationship between $F_{t,a}/F_{n,m}$ and d_{slip} in a constant normal force experiment and variable normal force experiment. For the constant normal force experiment, $F_{t,a}/F_{n,m}$ increases with the increase of $F_{n,a}$, but when $F_{t,a}/F_{n,m}$ is equal to the slip friction coefficient, it will no longer increase, but remain a constant. But for the variable normal force experiment, when $F_{t,a}/F_{n,m}$ is greater than the friction coefficient, the fluctuation of normal force will lead to an increase of $F_{t,a}/F_{n,m}$. It should be noted that when $F_{t,a}/F_{n,m}$ is less than the friction coefficient, the fluctuation of normal force will cause d_{slip} to increase. Fig-

ure 8(d) shows the logarithmic relationship between $F_{t,a}/F_{n,m}$ and energy dissipation E_D in the constant normal force experiment and variable normal force experiment. The relationship between E_D and $F_{t,a}/F_{n,m}$ is the same as that between d_{slip} and $F_{t,a}/F_{n,m}$. It should be noted that when $F_{t,a}/F_{n,m}$ is less than the friction coefficient, the fluctuation of normal force will lead to an increase of energy dissipation.

In this experiment, the conclusion of Asai *et al.*'s metal material is verified by using polymer material. After finite element analysis, Asai *et al.*[12] thought that this phenomenon is caused by the fluctuation of normal force and the change of stress distribution of interface contact force. Then we use the method mentioned in Subsection 3.1 to analyze the stress distribution in the vibration process.

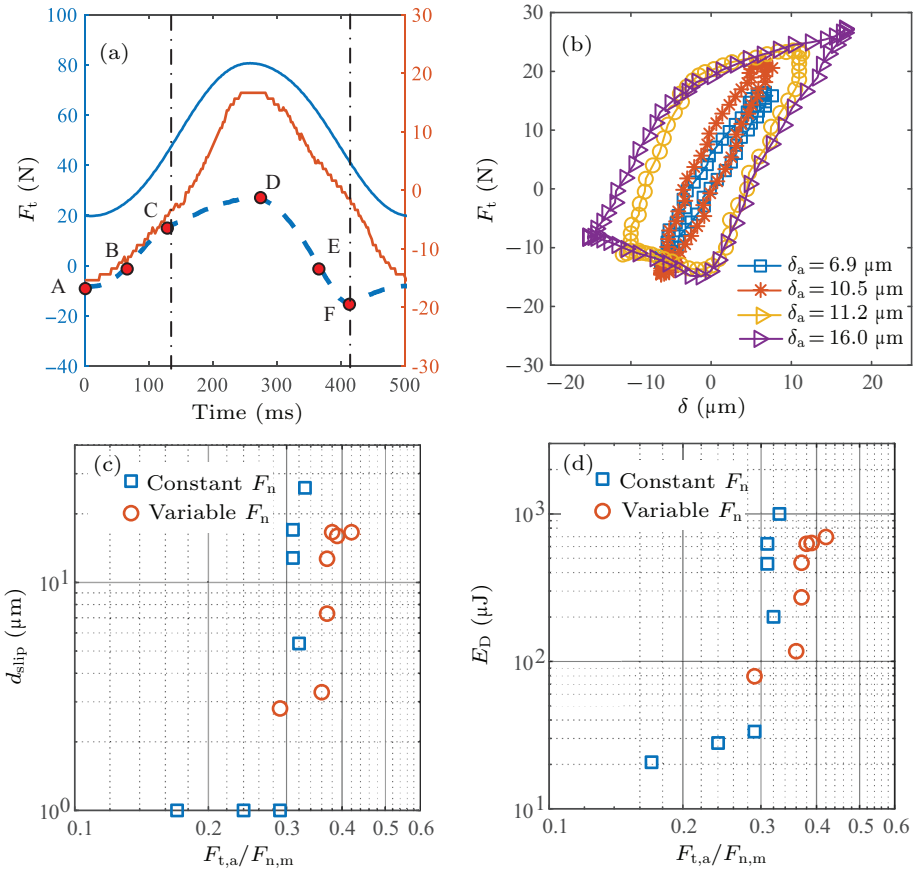


Fig. 8. Experimental results of variable normal force. (a) Time history curve of one cycle of F_t, F_n, and δ; (b) hysteretic curves of different δ_a; (c) relation curve between δ_a and d_{slip}; and (d) relation curve between δ_a and E_D.

3.3. Micro sliding friction behavior in experiments with different vibration angles

The vibration angle α can be controlled by adjusting $F_{n,a}/F_{t,a}$, and it is called vibration angle experiment. Set $F_{n,m} = 50$ N and $F_{n,a}/F_{t,a}$ to 0.1, 0.3, 0.5, 0.8, 1.0, and 1.7, separately, and the corresponding vibration 5°, 15°, 28°, 38°, 45°, 60°. The relative error of the maximum tangential force is less than 3.3%. When vibration angles are 5°, 38°, 45°, and 60°, the corresponding hysteresis curves are shown in Fig. 9(a). When the vibration angle exists, the hysteretic curve is no longer symmetrical about the center point. With the increase of vibration angle, the hysteretic curve gradually increases, and the hysteretic curve gradually shifts upward. With the increase in vibration period, one side of the interface is easier to wear, which is also verified by the observation of the surface wear area after the experiment. Figure 9(b) shows the corresponding relationship curve between $\delta$and F_t/F_n. It is noticeable that the friction coefficient of the positive slip section remains almost unchanged, but the friction coefficient of the negative slip section changes significantly. The friction coefficient increases with the increase of vibration angle when the vibration angle is 45°. When the vibration angle is 45°, the negative friction coefficient increases by 20%. The negative friction coefficient increases by 32%. The values of tangential stiffness $K_{t,p}$ and $K_{t,n}$ at different vibration angles are calculated, and the results are shown in Fig. 9(c). When the vibration angle is less than 38°, the values of $K_{t,p}$ and $K_{t,n}$ are almost equal. When the vibration angle is greater than 38°, $K_{t,p}$ decreases with the increase of vibration angle, but $K_{t,n}$ increases with the increase of vibration angle, and the difference between $K_{t,n}$ and $K_{t,p}$ increases with the increase of vibration angle. With the increase of vibration angle, the proportion of positive stick segment in positive segment decreases gradually. The relationship between vibration angle and d_{slip} is shown in

Fig. 9(d). The value of d_{slip} decreases with the increase of vibration angle. When $\alpha > 38°$, d_{slip} decreases faster. The experimental results provide a basis for us to improve the friction model considering the hysteresis of the friction coefficient.

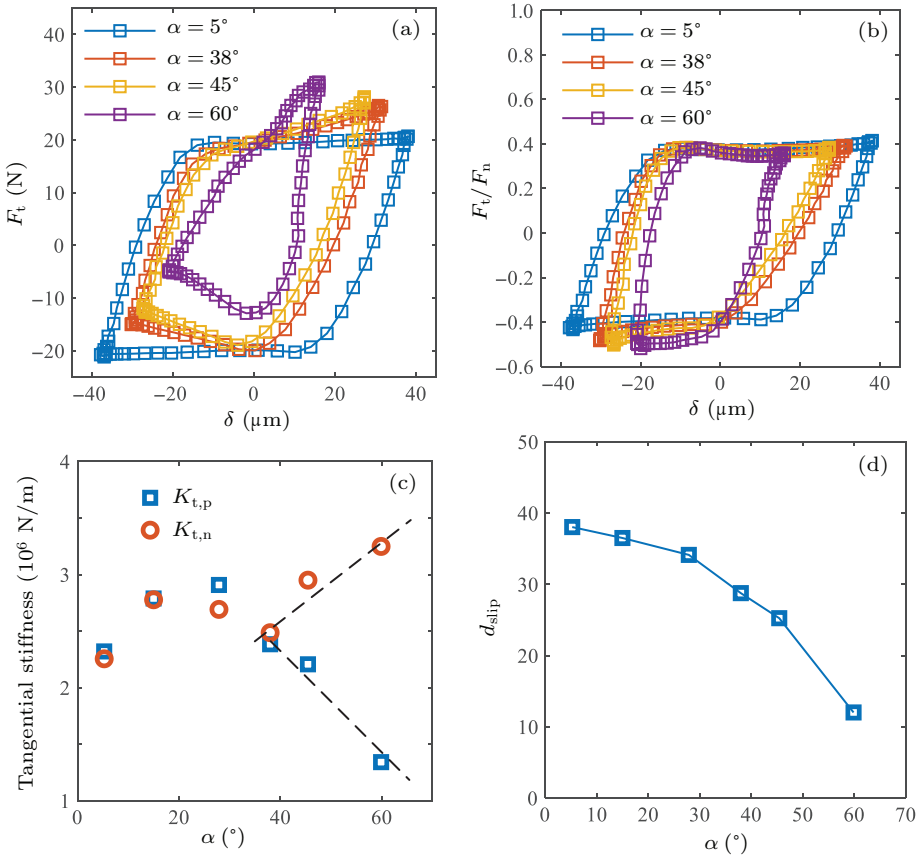


Fig. 9. Vibration angle experiment. (a) Hysteretic curve at different vibration angles. (b) Relation curves of F_t/F_n and δ for different vibration angles. (c) Relationship curve between tangential stiffness and α. (d) Relation curve between d_{slip} and vibration angle.

3.4. Influence of normal force fluctuation on interface stress distribution

To use a discrete mathematical model to simulate the stress distribution, the contact area is divided into 10 parts along the X direction and denoted by D_i as shown in Fig. 9(a). Referring to formula (3), the intensity ratio of the local contact image is calculated as the equivalent stress distribution $\bar{P}(i,t)$, $i = 1,2,\ldots,10$. The change of $\bar{P}(i,t)$ with time is shown in Fig. 9(b), and the change of image after applying excitation has good repeatability. The δ_0, $\delta_{\max}$, and $\delta_{\min}$ represent 0, maximum, and minimum of δ, respectively. Refer to formula (3), then $\bar{P}(i,t)$ at δ_0 will be taken as the standard. The normalized equivalent stress distributions $\bar{P}_s(i,t_{\delta_0})$, $\bar{P}_s(i,t_{\delta_{\max}})$, $\bar{P}_s(i,t_{\delta_{\min}})$ are calculated for δ_0, $\delta_{\max}$, and $\delta_{\min}$. The change of constant normal force $\bar{P}_s(i,t)$ is shown in Fig. 9(c). When $\delta = \delta_{\max}$, the maximum normal stress appears at the front end of the contact interface. When $\delta = \delta_{\min}$, the maximum normal stress occurs at the rear end of the contact interface. The change of stress distribution is mainly reflected from the two ends of the contact interface. In the constant normal stress experiment, the change of stress distribution is small. The change of $\bar{P}_s(i,t)$ when the normal force changes is shown in Fig. 9(d). The $\bar{P}_s(i,t_{\delta_{\max}})$ is significantly higher than $\bar{P}_s(i,t_{\delta_0})$, and $\bar{P}_s(i,t_{\delta_{\min}})$ is significantly lower than $\bar{P}_s(i,t_{\delta_0})$. When the normal force fluctuates, the change of $\bar{P}_s(i,t)$ is much larger than when normal force is constant.

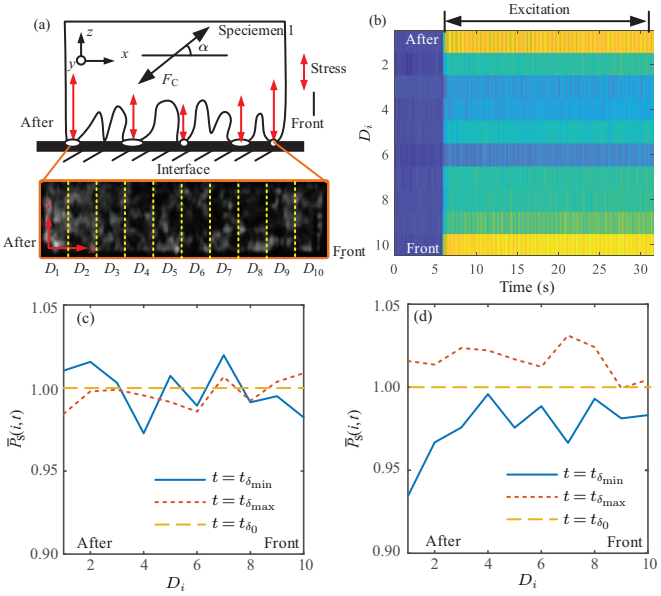


Fig. 10. Influences of normal force fluctuation on normal stress distribution of interface: (a) contact image, (b) $\bar{P}(i,t)$ changing with time, (c) variations of equivalent stress distribution $\bar{P}(i,t)$ with D_i at different time scales in the experiment of constant normal force, (d) variations of equivalent stress distribution at different time scales in the experiment of the variable normal force.

And the stress change at the back end of the contact area is greater than that at the front end. This shows that when the normal force fluctuates, the amplitude of stress distribution not only increases, but also varies at different positions of the contact area. This finding not only verifies the finite element analysis conclusion of Asai *et al.*,[12] but also obtains the dynamic stress distribution under the real contact condition, thereby providing an experimental basis for better revealing the mechanism of micro sliding friction behavior.

3.5. Influence of vibration angle change on interface stress distribution

In this subsection, the internal mechanism of this phenomenon is mainly analyzed through the evolution of stress distribution in the vibration process. When $\alpha = 5°$, $\bar{P}(i,t_{\delta_{\max}})$ and $\bar{P}(i,t_{\delta_{\min}})$ are shown in Fig. 11(a). It can be found that the normal stresses at both ends of the interface are the largest, and the stress at the back end is greater than that at the front end, but the stress distribution changes little in the whole vibration process. When $\alpha = 60°$, $\bar{P}(i,t_{\delta_{\max}})$ and $\bar{P}(i,t_{\delta_{\min}})$ are shown in Fig. 11(b). When the vibration angle is large, $\bar{P}(i,t_{\delta_{\max}})$ increases significantly and $\bar{P}(i,t_{\delta_{\min}})$ decreases significantly, and the fluctuation amplitude of stress distribution is larger at the back end of the interface than at the front end, which is consistent with the conclusion in Subsection 2.4. To compare the variation of fluctuation amplitude, the average value of $\bar{P}_s(i,t)$ is taken as the standard when $\alpha = 5°$, and the dimensionless fluctuation amplitude $\bar{P}_a(i)$ is calculated. When the vibration angles are 5°, 15°, 28°, 38°, 45°, and 60°, the distribution of $\bar{P}_a(i)$ is shown in Fig. 11(c). With the increase of vibration angle, $\bar{P}_a(i)$ increases, and $\bar{P}_a(i)$ at the rear end is larger than at the front end. Because $\bar{P}_a(i)$ changes approximately linearly along the x direction, the absolute value of its slope is called fluctuation unevenness λ_v. The larger the λ_v , the larger the difference between the front and back stress amplitude is and the more uneven the stress distribution. Figure 11(d) shows the calculations of λ_v at different angles. It can be found that when the vibration angle is less than 15°, λ_v increases rapidly with the increase of angle. The vibration angle is in a range from 15° to 45°, λ_v varies approximately linearly. When the vibration angle is greater than 45°, the growth rate of λ_v slows down. The experimental results show that when the normal force fluctuates, the fluctuation amplitude of the local stress distribution of the interface is not the same as when the normal force does not fluctuate. Asai *et al.*[12] believed that the uneven stress distribution caused by the fluctuation of the normal force is one of the reasons for the increase of energy dissipation. Based on the experimental data, a quantitative analysis method of uneven stress distribution is proposed, which provides an experimental basis for improving the friction model.

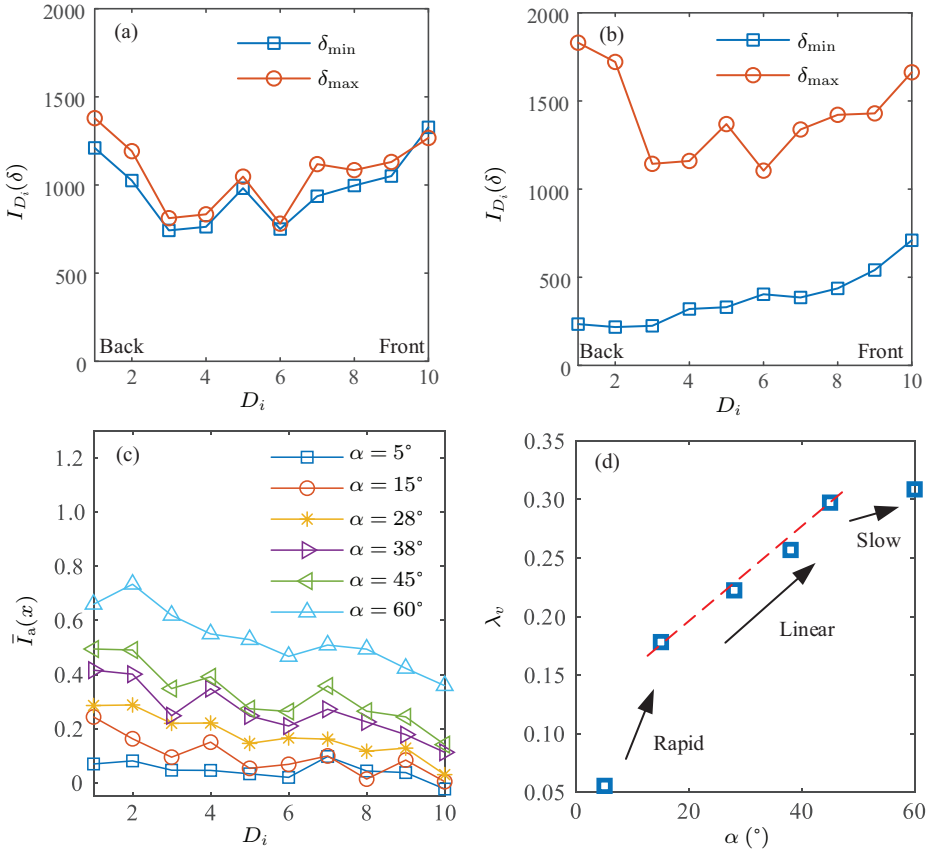


Fig. 11. Effects of vibration angle on stress distribution. (a) Stress distribution when $\alpha = 5°$, (b) stress distribution when $\alpha = 60°$, (c) fluctuation amplitude distributions for different vibration angles, and (d) relationship between the fluctuation unevenness and vibration angle.

4. Improved micro sliding friction model

4.1. Mechanism analysis of micro sliding friction behavior

Through the experimental analysis in Section 3, we find that when the normal force fluctuates, the hysteretic curve has the following four characteristics: first, the hysteretic curve is no longer symmetrical about the center point; second, the friction coefficient of the negative section is greater than that of positive section; third, the tangential stiffness of negative section is greater than that of positive viscous section; fourth, the fluctuation amplitude of stress distribution at the interface is not equal. We hope to build a mathematical model that can fully describe the above characteristics of the hysteresis curve and improve the accuracy of contact behavior prediction. Based on the Iwan model, the stress distribution is simulated by a limited number of Jenkins spring slider elements in parallel, and then the influence of stress distribution on contact parameters is considered. The improved Iwan model is shown in Fig. 12.

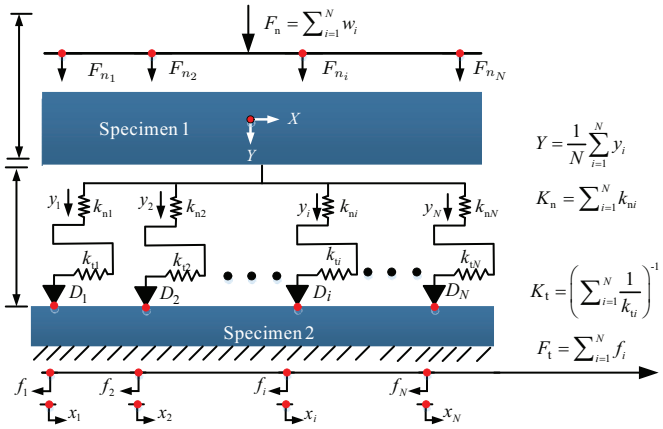


Fig. 12. Improved model considering the effect of stress distribution.

Specimen 1 and specimen 2 contact to form a contact interface. Specimen 2 is fixed, and normal force F_{n} and tangential force F_{t} are applied to specimen 1. The tangential displacement of specimen 1 is X and the normal displacement is Y, which are expressed by Eqs. (4) and (5), respectively. Because the load distribution at the contact interface is mainly determined by the contact asperity, we use n Jenkins elements to simulate the uneven normal force on the local area, and F_{n_i} is the normal force on the Jenkins element in the order of i. Each Jenkins element is composed of a normal spring and tangential spring with stiffness $k_{\mathrm{n}i}$ and $k_{\mathrm{t}i}$, respectively, and a damping slider D_i with coefficient $f_{\mathrm{c}i}$. The $k_{\mathrm{n}i}$ is called normal stiffness and $k_{\mathrm{t}i}$ is named tangential stiffness. In this model, the pseudo stiffness and the tangential stiffness act on D_i independently, and there is no coupling effect. The y_i is the compression of the normal spring under the action of F_{n_i}, x_i and f_i are the displacement and friction of D_i. The friction F_{t} of interface is the sum of friction f_i of all D_i, which is expressed by formula (6).

The critical friction F_{c} of the interface is the sum of the critical friction $f_{\mathrm{c}i}$ of all D_i, as shown in formula (7).

$$X = X_{\mathrm{m}} + X_{\mathrm{a}} \sin(2\pi w t), \tag{4}$$

$$Y = Y_{\mathrm{m}} + Y_{\mathrm{a}} \sin(2\pi w t), \tag{5}$$

$$F_{\mathrm{t}} = \sum_{i=1}^{N} f_i, \tag{6}$$

$$F_{\mathrm{c}} = \sum_{i=1}^{N} f_{\mathrm{c}i}. \tag{7}$$

According to the characteristics of the hysteretic curve, it is divided into the positive segment and negative segment, in which positive and negative refer to the direction of relative displacement. The positive segment includes positive viscosity and positive sliding, and the negative segment includes negative viscosity and negative sliding. The four contact states are shown in Fig. 13. The state transition points of each stage are represented by ${}_{\mathrm{sub_l}}C^{\mathrm{sup}}_{\mathrm{sub_r}}$, in which the superscript (sup) represents the direction of displacement u at the present time, the right subscript ($\mathrm{sub_r}$) represents the state at the next time, and the left subscript ($\mathrm{sub_l}$) represents the state at the previous time. There are four state transition sequences for viscous state and sliding state. The four state transition points are represented by ${}_{\mathrm{slip}}C^{\mathrm{P}}_{\mathrm{stick}}$, ${}_{\mathrm{stick}}C^{\mathrm{P}}_{\mathrm{slip}}$, ${}_{\mathrm{slip}}C^{\mathrm{N}}_{\mathrm{stick}}$, and ${}_{\mathrm{stick}}C^{\mathrm{N}}_{\mathrm{slip}}$, and the point with zero friction is called friction 0 point, It is also often used in vibration analysis, which is expressed by C^{P}_0 and C^{N}_0 according to the direction of motion.

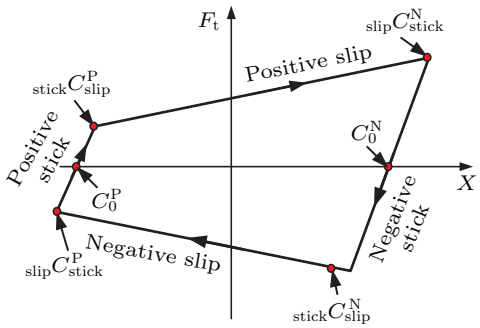


Fig. 13. State transition sequence.

It should be noted that considering the hysteresis of friction, the direction of friction f_i at the point D_i in this model is calculated according to the direction of acceleration. The transition criteria of four states are shown in formula (8), and are expressed in formula (9). In the formula, $x_{i,\mathrm{rev}}$ and $f_{i,\mathrm{rev}}$, respectively, represent the displacement and friction at a state speed of 0 at the point D_i.

$$\begin{aligned}
&{}_{\mathrm{stick}}C^{\mathrm{P}}_{\mathrm{slip}} : f_{\mathrm{t}i}(t) \geq f_{\mathrm{c}i}(t) \ \text{ and } \ k_{\mathrm{t}i}(t)\dot{X}(t) - \dot{f}_{\mathrm{c}i}(t) > 0,\\
&{}_{\mathrm{stick}}C^{\mathrm{N}}_{\mathrm{slip}} : f_{\mathrm{t}}(t) \leq -f_{\mathrm{c}i}(t) \ \text{ and } \ k_{\mathrm{t}i}(t)\dot{X}(t) + \dot{f}_{\mathrm{c}i}(t) < 0,\\
&{}_{\mathrm{slip}}C^{\mathrm{P}}_{\mathrm{stick}} : \dot{X}(t) + \dot{f}_{\mathrm{c}i}(t)/k_{\mathrm{t}i}(t) \geq 0 \ \text{ and } \ \ddot{X}(t) + \ddot{f}_{\mathrm{c}i}(t)/k_{\mathrm{t}i}(t) > 0,\\
&{}_{\mathrm{slip}}C^{\mathrm{N}}_{\mathrm{stick}} : \dot{X}(t) - \dot{f}_{\mathrm{c}i}(t)/k_{\mathrm{t}i}(t) \leq 0 \ \text{ and } \ \ddot{X}(t) - \ddot{f}_{\mathrm{c}i}(t)/k_{\mathrm{t}i}(t) < 0,
\end{aligned} \tag{8}$$

$$f_i = \begin{cases} f_{ci}, & {}_{\text{stick}}C^{\text{P}}_{\text{slip}} \to {}_{\text{slip}}C^{\text{N}}_{\text{stick}}, \\ -f_{ci}, & {}_{\text{stick}}C^{\text{N}}_{\text{slip}} \to {}_{\text{slip}}C^{\text{P}}_{\text{stick}}, \\ k_{ti}(X(t) - x_{i,\text{rev}}) + f_{i,\text{rev}}, & {}_{\text{slip}}C^{\text{P}}_{\text{stick}} \to {}_{\text{stick}}C^{\text{P}}_{\text{slip}}, \\ k_{ti}(X(t) - x_{i,\text{rev}}) + f_{i,\text{rev}}, & {}_{\text{slip}}C^{\text{N}}_{\text{stick}} \to {}_{\text{stick}}C^{\text{N}}_{\text{slip}}. \end{cases} \tag{9}$$

4.2. Micro sliding friction behavior based on equivalent stress distribution

Figure 14 describes the whole micro sliding process based on the stress change. When the interface state is ${}_{\text{slip}}C^{\text{P}}_{\text{stick}}$, it indicates the starting point of positive viscosity as shown in Fig. 14(a). To simulate the characteristics of stress distribution, the deformation, red dot, and line shape of the tangential spring are used to represent the contact states. The deformation of spring represents the shear force at this point. The shear force increases with the increase of deformation. The red dot and line shape represent the normal force. The red dot represents the area with a larger tangential load. The dashed line segment and the pointed line segment indicate that the friction decreases gradually. It should be noted that when the initial normal stress is uniformly contacted, the linear distribution can be used as the equivalent stress distribution to simulate the gradual disconnection process of D_i with the increase of tangential force, which is easy to understand when the tangential force is loaded unidirectionally. However, when the tangential force moves back and forth, once the tangential force reverses the direction, the equivalent stress should also reverse accordingly, which will bring us trouble when modeling in a fixed order D_i. Considering that Jenkins elements are parallel, the order of D_i does not affect the calculation of tangential force.

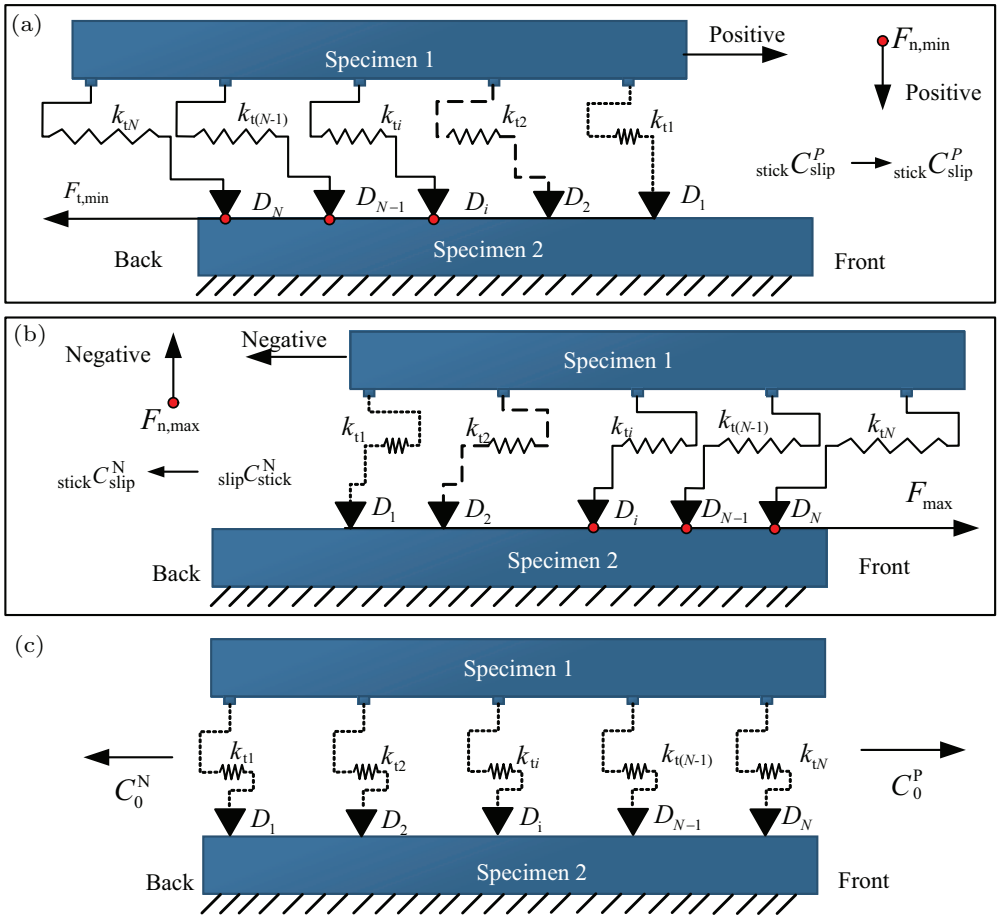


Fig. 14. Simulation of micro sliding process.

Therefore, the following description, D_i does not describe the placement order on the interface, but only for the magnitude of the tangential force. The larger, the value of i, the greater the tangential stress is. In the process of movement, the normal stress and the tangential stress are positively correlated with each other. In the following description, stress is used to represent the change of tangential stress. Assuming that the initial state of the interface is ${}_{\text{slip}}C^{\text{P}}_{\text{stick}}$ as shown in Fig. 14, the stress at the back end of the interface is greater than at the front end, the deformation decreases from D_N to D_1 and then decreases in turn, and the deformation of D_1 is the smallest, which is due to the minimum critical friction. When $F_{\text{t}} = F_{\text{c}}$, specimen 1 begins to slide, the interface is in ${}_{\text{stick}}C^{\text{P}}_{\text{slip}}$ state, and the interface stress remains stable until it reaches ${}_{\text{slip}}C^{\text{N}}_{\text{stick}}$, currently, displacement X, normal load F_{n} and tangential load F_{t} reach the maximum. Then the tangential load starts to move

in the opposite direction as shown in Fig. 14(b). It should be noted that at this time, the equivalent stress distribution of the interface turns over instantaneously, and the stress at the front end of the interface is greater than that at the back end. Under the action of the tangential load, the interface state changes in the order of ${}_{\text{slip}}C^{\text{N}}_{\text{stick}}$–${}_{\text{stick}}C^{\text{N}}_{\text{slip}}$–${}_{\text{slip}}C^{\text{N}}_{\text{stick}}$. Except for the opposite direction, other motion modes of the interface are the same as before and will not be repeated. There is also a special state point C^{N}_0 and C^{P}_0, as shown in Fig. 14(c), which may appear in the sliding or viscous process. At this time, the friction force is 0, which is called the zero point of friction.

4.3. Contact parameter fluctuation caused by normal force fluctuation

In the simulation analysis of Subsection 4.2, the linear distribution is used to be equivalent to the stress distribution, but in fact, the normal stress distribution is not uniform due to machining error, assembly error, or the requirements for experimental conditions. We also verify this phenomenon experimentally in Section 3, then we use the power function $P(i,a)$ to describe the variation of the equivalent stress distribution as shown in formula (10). The characteristic of this function is that it can describe multiple distributions by adjusting the value of a as shown in Fig. 15(a). The $P(i,0)$ refers to the uniform distribution, $P(i,1)$ is the linear distribution, $P(i,a<1)$ represents the slower growth of stress distribution, $P(i,a>1)$ denotes faster growth of stress distribution. The larger the a value, the more uneven the stress distribution is. Formula (11) can be used to express the non-uniform fluctuation of equivalent stress distribution caused by the fluctuation of the normal force. According to formulas (10) and (11), the equivalent load F_{n_i} of D_i point in the process of micro sliding can be deduced as shown in formula (12).

$$P(i,a) = i^a \left(\sum_{i=1}^{N} i^a \right)^{-1}, \tag{10}$$

$$a = a_{\text{m}} + a_{\text{a}} \sin(2\pi wt), \tag{11}$$

$$F_{n_i} = k_{\text{n}i} F_{n_{i,\text{m}}} P(i,a) \left(1 + R_{\text{w}} \sin(2\pi wt)\right), \tag{12}$$

where $P(i,a)$ is the stress distribution function, a_{m} and a_{a} are the mean value coefficient and amplitude coefficient of the stress distribution function, and R_{w} is the normal force fluctuation coefficient.

In the vibration angle experiment, we find that the tangential stiffness is not a constant. When the vibration angle is greater than 40°, K_{t} fluctuation will have a significant effect on the hysteresis curve, and increase with vibration angle increasing. Based on the above analysis, K_{t} at different vibration angles can be expressed by formula (13), R_{K} is the stiffness fluctuation coefficient, $K_{\text{t,m}}$ is a function and is correlated linearly with $F_{\text{n,m}}$, and formula (14) is used. The friction coefficient has similar characteristics. In the positive section, the friction coefficient is μ_{p} and the negative friction coefficient is μ_{n}. They are related by formula (15). R_μ is a function related to R_{na}, as shown in formula (16).

$$K_{\text{t}} = \begin{cases} K_{\text{t,m}}\left(1 + R_{\text{K}} R_{\text{na}} \sin(2\pi wt)\right), & R_{\text{na}} \geq 0.84\mu, \\ K_{\text{t,m}}(1 - R_{\text{K}} R_{\text{na}}), & R_{\text{na}} < 0.84\mu, \end{cases} \tag{13}$$

$$K_{\text{t,m}} = p_1 F_{n,m} + p_2, \tag{14}$$

$$\mu_{\text{n}} = R_\mu \mu_{\text{p}}, \tag{15}$$

$$R_\mu = \begin{cases} p_3 R_{\text{na}} + p_4, & R_{\text{na}} \geq 0.84\mu, \\ 1, & R_{\text{na}} < 0.84\mu, \end{cases} \tag{16}$$

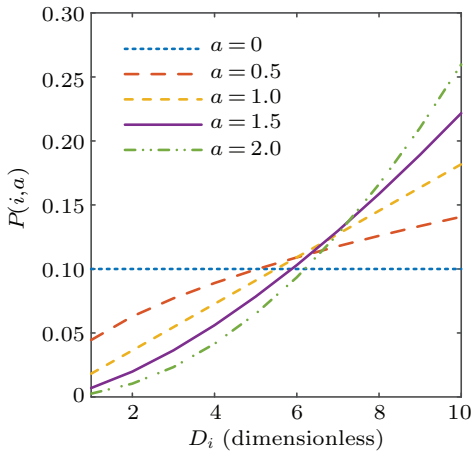


Fig. 15. Equivalent stress distribution based on exponential function.

4.4. Calculation process and case verification

The flowchart of friction calculation is shown in Fig. 16. Firstly, the relevant contact parameters are identified according to the experimental results, including normal force mean value $F_{\text{n,m}}$, normal force fluctuation coefficient R_{na}, positive friction coefficient μ_{n}, negative friction coefficient μ_{p}, displacement fluctuation amplitude X_{a}, tangential stiffness mean value $K_{\text{t,m}}$, tangential stiffness fluctuation coefficient R_{K}, excitation frequency w, and tangential stress distribution coefficient a_{m} and a_{a}. All parameters of the model have clear physical meanings and can be identified by experimental results. By adjusting the number of Jenkins cells, it can achieve faster simulation. By adjusting the contact parameters, it can be used to analyze the influence of contact parameters on the hysteretic curve, and then analyze the changes of damping and energy dissipation under the fluctuation of the normal force.

Taking the experiment with vibration angle $\alpha = 60°$ for example, some parameters are expressed as follows: $F_{\text{n,m}} = 81$ N, $F_{\text{n,a}} = 61$ N, $K_{\text{t,p}} = 2.3 \times 10^6$ N/m, $R_{\text{na}} = 0.58$, $K_{\text{t,n}} = 5.0 \times 10^6$ N/m, $\mu_{\text{n}} = 0.41$, $\mu_{\text{p}} = 0.33$, and $\lambda_v = 0.31$.

The comparison between the predicted values of the friction model and the experimental results is shown in Fig. 17.

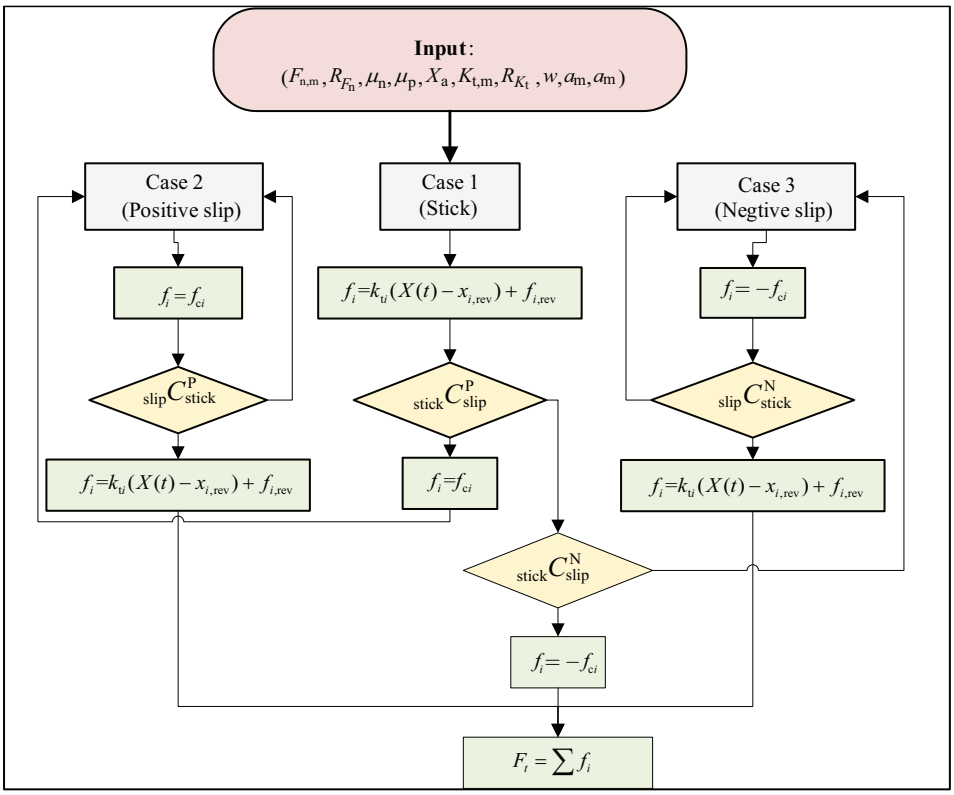


Fig. 16. Flowchart of friction model.

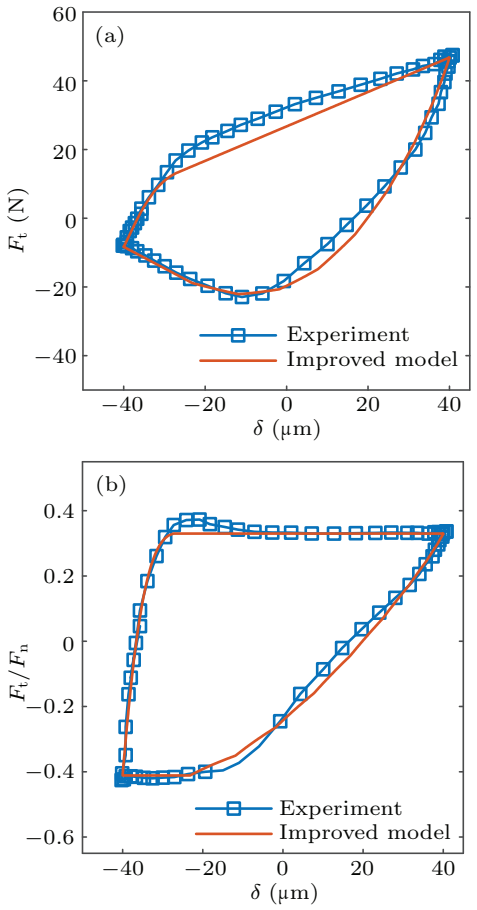


Fig. 17. Comparison between theoretical results and experimental results. (a) Hysteresis curve and (b) relationship curve between F_t/F_n and δ.

In the experiment of Subsection 2.2, the influences of normal force fluctuation on energy dissipation are compared. It is found that when $F_{t,a}/F_{n,m}$ is greater than the friction coefficient, the energy dissipation is less than when the normal force is constant; however, when $F_{t,a}/F_{n,m}$ is less than the friction coefficient, the energy dissipation will need to consider the fluctuation of the normal force. In this subsection, the mathematical model is used to analyze the mechanism of this phenomenon. The $F_{t,a}/F_{n,m}$ is referred to as alternating friction coefficient, which is expressed by R_{tanm}. By adjusting the parameters, the hysteretic curve and energy dissipation of friction force corresponding to the fluctuation of normal force and constant normal force are calculated. When the normal force fluctuates, the value of A is adjusted, separately, to $[5, 8, 10, 15, 20, 30, 40] \times 10^{-6}$ m, $R_{na} = 0.6$. When the normal force is constant, the value of A is adjusted, separately, to $[3, 5, 7, 10, 15, 20, 30, 40] \times 10^{-6}$ m, $R_{na} = 0$. It should be noted that only when considering the fluctuation of normal force, will R_{tanm} be greater than the sliding friction coefficient μ, otherwise $R_{tanm} \leq \mu$. Figures 18(a) and 18(b) show the hysteresis curves corresponding to different values of $F_{t,a}/F_{n,a}$ when the normal force fluctuates and when the normal force is constant.

It can be found that when $R_{tanm} \leq \mu$, the area enclosed by the hysteretic curve increases due to the fluctuation of the normal force, which is mainly due to the stress distribution leading the tangential stiffness to slow down gradually with the increase of the tangential force. When the normal force

fluctuates, the larger the normal force, the larger the tangential stiffness of the negative viscous section is, which results in the larger deformation of the negative section curve, thereby increasing the energy dissipation. Figure 18(c) shows the energy dissipation of different values of R_{tanm} in two cases: constant normal force and variable normal force. When $R_{\text{tanm}} \leq \mu$, considering the fluctuation of normal force, the energy dissipation is less than the value when the normal force is constant; when $R_{\text{tanm}} > \mu$, the energy dissipation of normal force fluctuation is larger than that of constant normal force, which is consistent with the experimental phenomenon. This is the first time that this phenomenon has been explained based on the fluctuation of stress distribution. Figure 18(d) shows the energy dissipations for different driving displacements under constant normal force and variable normal force. When the driving displacement is small, the fluctuation of normal force can cause greater energy dissipation. When the driving displacement is large, the influence of normal force fluctuation on energy dissipation is small. It should be noted that this phenomenon mainly occurs in the heavy load contact of soft materials or hard materials. Because the tangential stress distribution of softer material fluctuates more obviously with the fluctuation of normal force, the distribution of harder material (stainless steel) is mainly linear under light load. Only under heavy load, will the stress distribution show obvious uneven fluctuation, which will affect the change of energy dissipation. Based on the above analysis, we have reason to think that the theory can be used in the vibration analysis of blade dampers.

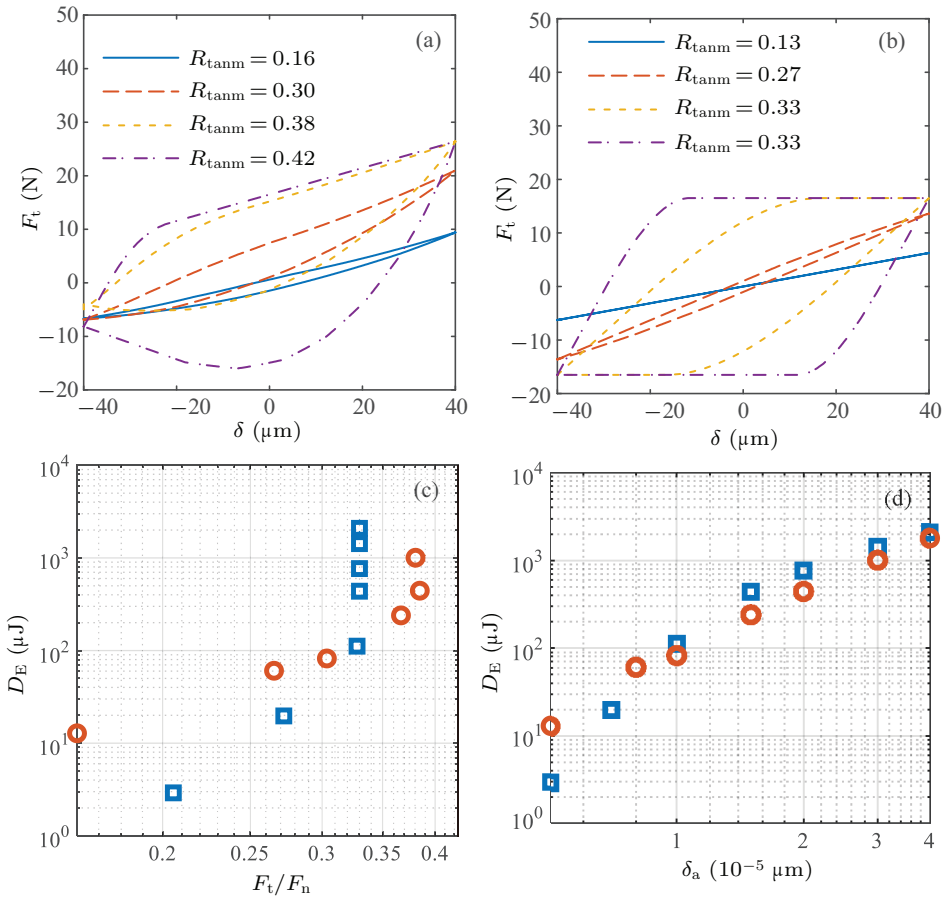


Fig. 18. Energy dissipation. (a) Hysteretic curves of different values of R_{tanm} in variable normal force experiment, (b) hysteretic curves of different values of R_{tanm} in constant normal force experiment, (c) logarithmic graph of R_{tanm} and energy dissipation, and (d) logarithmic graph of δ_{a} and energy dissipation.

5. Conclusions

In this work, based on the experimental analysis, a micro sliding friction model considering the influence of stress distribution fluctuation is established. The main conclusions are as follows.

(i) The fluctuation of normal force will lead to hysteresis of friction coefficient. The friction coefficient of the negative sliding section is greater than that of the positive sliding section. When the normal force is constant, the energy dissipation increases linearly with the increase of relative displacement amplitude, and the contact interface stress has little effect on the linear relationship. When the ratio of the amplitude of tangential force to the initial value of normal force is larger than the friction coefficient, the fluctuation of normal force will lead the sliding distance d_{slip} and energy dissipation E_{D} to decrease, which will be more obvious with the increase in the ratio of the amplitude of tangential force to initial value of normal force; when the ratio of the amplitude of tangential

force to initial value of normal force is less than the friction coefficient, the fluctuation of normal force will result in greater energy dissipation; the fluctuation of normal force will cause the interface stress distribution to fluctuate unevenly.

(ii) The vibration angle will reduce the sliding distance and energy dissipation, and cause and negative tangential stiffness to no longer equal. The difference between positive tangential stiffness and negative tangential stiffness will increase with vibration angle increasing. The uneven fluctuation of stress will lead the energy dissipation to decrease (increase) when the ratio of the amplitude of tangential force to the initial value of normal force is greater (less) than the friction coefficient .

(iii) A micro sliding friction model considering the fluctuation of contact parameters caused by the fluctuation of stress distribution is established. This friction model considers the interface shear stiffness fluctuation, friction coefficient lag, and uneven stress distribution fluctuation. This model can be used to analyze the influence of various nonlinear contact parameters on contact behavior. By comparing the experimental results with the simulation results of proposed model, we find that considering the nonlinear effect of a certain contact parameter alone may bring greater error to the prediction of friction. The accuracy of friction prediction can be improved by integrating multiple contact parameters.

Acknowledgements

The authors wish to thank Mr. Kawamura for his encouragement of this study.

Project supported by the National Natural Science Foundation of China (Grant No. 11872033) and the Beijing Natural Science Foundation, China (Grant No. 3172017).

References

[1] Sextro W 2000 *Proceedings of the ASME Turbo Expo* 2000*: Power for Land, Sea, and Air* Education, May 8–11, 2000, Munich, Germany, V004T03A067
[2] Usta A D, Shinde S and Eriten M 2017 *J. Tribol.* **139** 061402
[3] Gu W W and Xu Z L 2010 *Proceedings of the ASME Turbo Expo* 2010*: Power for Land, Sea, and Air*, June 14–18, 2010, Glasgow, UK, p. 809
[4] Eriten M, Lee C H and Polycarpou A A 2012 *Tribol. Int.* **50** 35
[5] Pesaresi L, Armand J, Schwingshackl C W, Salles L and Wong C 2018 *J. Sound Vib.* **436** 327
[6] Xiao H, Shao Y and Xu J 2014 *Eur. J. Mech.-A Solids* **43** 1
[7] Goodman L E 1980 *Applied Mechanics Division, AMD*
[8] Capozza R and Urbakh M 2012 *Phys. Rev. B* **86** 085430
[9] Daniel J, Segalman D J and Danny L 2009-07-01, Sandia National Laboratories: Sandia National Laboratories.
[10] Pesaresi L, Salles L, Elliott R, Jones A, Green J S and Schwingshackl C W 2016 *AMM* **849** 1
[11] Pesaresi L, Salles L, Jones A, Green J S and Schwingshackl C W 2017 *Mech. Syst. Signal Processing* **85** 662
[12] Asai K and Gola M M 2015 Proceedings of the ASME Turbo Expo 2015: *Turbine Technical Conference and Exposition*, June 15–19, 2015, Quebec, Canada, V07BT33A002
[13] Campañá C, Persson B N J and Müser M H 2011 *J. Phys.: Condens. Matter* **23** 085001
[14] Parker R C and Hatch D 1950 *Proc. Phys. Soc. B* **63** 185
[15] Bhushan B 1985 *A S L E Trans.* **28** 181
[16] Müser M H, Dapp W B, Bugnicourt R, Sainsot P, Lesaffre N, *et al.* 2017 *Tribol. Lett.* **65** 118
[17] Yamaguchi T, Sawae Y and Rubinstein S M 2016 *Extreme Mech. Lett.* **9** 331
[18] Dillavou S and Rubinstein S M 2018 *Phys. Rev. Lett.* **120** 224101
[19] Matsukawa H, Otsuki M and Nakano K 2015 *J. Surf. Sci. Soc. Jpn.* **36** 222
[20] Otsuki M and Matsukawa H 2013 *Sci. Rep.* **3** 1586
[21] Kato A, Obara K, Igarashi T, Tsuruoka H, Nakagawa S and Hirata N 2012 *Science* **335** 705
[22] Ozaki S, Mieda K, Matsuura T and Maegawa S 2018 *Lubricants* **6** 38
[23] Maegawa S, Itoigawa F and Nakamura T 2016 *Tribol. Int.* **93** 182
[24] Maegawa S, Itoigawa F and Nakamura T 2016 *Tribol. Lett.* **62** 1
[25] Sanliturk K Y and Ewins D J 1996 *J. Sound Vib.* **193** 511
[26] Luo Z, Song B, Han J and Yan S 2019 *Chin. Phys. B* **28** 104601
[27] Luo Z, Song B, Han J and Yan S 2019 *Chin. Phys. B* **28** 054601
[28] Han J, Ding J, Wu H and Yan S 2022 *Chin. Phys. B* **31** 034601
[29] Lee H G, Yoon H M and Lee J S 2019 *Appl. Surf. Sci.* **481** 1573
[30] Tian K W, Nitya N G, David L G and Robert W C *J. Phys. Chem. B* **122** 991
[31] Han J, Luo Z, Zhang Y and Yan S 2022 *Chin. Phys. B* **30** 054601